Journal of Rock Mechanics and Geotechnical Engineering. 2012, 4 (2): 183–192

Journal of Rock Mechanics and Geotechnical Engineering

Journal online: www.rockgeotech.org

Numerical thermo-hydro-mechanical modeling of compacted bentonite in China-mock-up test for deep geological disposal

Liang Chen[1, 2*], Ju Wang[1, 2], Yuemiao Liu[1, 2], Federic Collin[3], Jingli Xie[1, 2]

[1] *Beijing Research Institute of Uranium Geology (BRIUG), Beijing, 100029, China*

[2] *CNNC Key Laboratory on Geological Disposal of High-level Radioactive Waste, Beijing, 100029, China*

[3] *Departement GeomaC, University of Liege, Sart Tilman B52/3, Chevreuils Road, 1, B-4000, Liege, Belgium*

Received 30 June 2011; received in revised form 11 November 2011; accepted 25 November 2011

Abstract: The China-mock-up test is to evaluate the performance of the compacted Gaomiaozi (GMZ) bentonite under coupled thermo-hydro-mechanical (THM) conditions in deep geological disposal. A numerical study of the test is conducted in this paper. The principal THM characteristics of the bentonite are presented at first. A THM model is then presented to tackle the complex coupling behavior of the bentonite. The model of Alonso-Gens is incorporated to reproduce the mechanical behavior of the bentonite under unsaturated conditions. With the proposed model, numerical simulations of the China-mock-up test are carried out by using the code of LAGAMINE. The time variations associated with the temperature, degree of saturation, suction and swelling pressure of the compacted bentonite are studied. The results suggest that the proposed model is able to reproduce the mechanical behavior of the bentonite, and to predict moisture motion under coupled THM conditions.

Key words: radioactive waste disposal; GMZ bentonite; thermo-hydro-mechanical (THM) modeling; China-mock-up test

1 Introduction

Deep geological disposal is a widely accepted concept for the high-level radioactive waste (HLW). In China, the research work on HLW disposal started in 1985. It had a plan to build a national repository by the middle of the 21st century. At present, the preliminary concept of HLW repository in China is a shaft-tunnel structure, located in saturated zones in granites, as shown in Fig. 1.

According to this concept, the engineered barrier system (EBS) comprises the vitrified waste, waste canisters, buffer materials, backfill and seals. Like many other countries, unsaturated compacted bentonite is foreseen in China as the best candidate for buffer material. Its low hydraulic conductivity, micro-porous structure, good sorption properties and swelling capacity make this material an effective barrier (Wersin et al., 2007). Currently, the Gaomiaozi (GMZ) bentonite has been preselected as the candidate buffer material for the Chinese repository system through a national screening and comparison (Wang et al., 2006). Numerous experimental investigations on the mineralogy and chemical composition, and the behaviors of the GMZ bentonite under the coupled physico-mechanical conditions have been performed

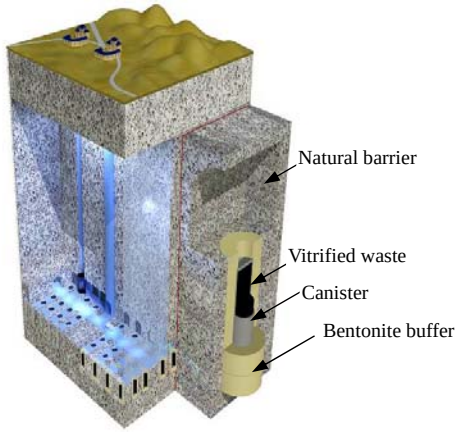

Fig. 1 Preliminary concept of HLW repository in China (Wang, 2010).

Doi: 10.3724/SP.J.1235.2012.00183

*Corresponding author. Tel: +86-13466678227;
E-mail: liangchencn@yahoo.cn

(Wen, 2005; Liu et al., 2007a, 2007b; Ye et al., 2010).

In order to further understand the performance of the GMZ bentonite under coupled THM conditions, a mock-up facility, named China-mock-up, has been installed in Beijing Research Institute of Uranium Geology (BRIUG). The heater, which substitutes a loaded waste canister, is placed inside of the facility. Water inflow through the barrier from its outer surface is also possible to simulate the intake of groundwater. In the paper, the basic physical characteristics of the GMZ bentonite and the experimental facility are introduced. Numerical simulations are carried out by the program LAGAMINE developed at University of Liege (Charlier, 1987). In the simulations, the following physical phenomena are taken into account: the transport of liquid (advection) and heat (convection and conduction), the vapor diffusion, and the evaporation and condensation phenomena of water. The constitutive model of Alonso-Gens (Alonso et al., 1990) is employed to reproduce the fundamental mechanical features of the GMZ bentonite in partially saturated condition.

Due to the lack of experimental data at present, a qualitative analysis of the predictive results is realized. It is suggested that the THM phenomena of compacted bentonite can be well reproduced and interpreted by the proposed model.

2 Basic THM properties of GMZ bentonite

The GMZ bentonite is taken from the Inner Mongolia Autonomous Region, 300 km northwest from Beijing, China. The advances in the knowledge of the physico-mechanical properties of the GMZ bentonite are reported in Ye et al. (2010). In this section, only the principal THM characteristics are summarized.

The thermal conductivity of the GMZ bentonite is found to increase as the dry density and water content increase (Liu et al., 2007a, 2007b). As far as the hydraulic properties are concerned, the water retention curve at room temperature under confined and unconfined conditions was obtained by Chen et al. (2006). The influence of temperature on the soil-water characteristics of highly compacted GMZ bentonite was also investigated by Ye et al. (2009a, 2009b). It is revealed that the water retention capacity of the highly compacted GMZ bentonite decreases as the temperature increases. According to the hydraulic conductivity study carried out by Wen (2006), the saturated hydraulic conductivity of the saturated GMZ bentonite decreases with the increase in dry density and temperature.

The mechanical behaviors of the GMZ bentonite are also investigated. For the same moisture content, the swelling velocity is revealed to increase with the increase in initial dry density, and the step-phase character of the curve will be more significant with the increase in dry density (Ye et al., 2007). The mechanical loading test at controlled suction and temperature is also carried out by Cui et al. (2011). An elastoplastic behavior with a clear change in slope is observed.

3 Coupled THM modeling

In order to reproduce the physico-mechanical behaviors of the GMZ bentonite aforementioned, a coupled THM model is proposed. In the model, various THM coupling phenomena are taken into account, including the transport of heat (conduction and convection), the motion of liquid water, the vapor diffusion, and their couplings with mechanical behaviors. The main formulations of the proposed model are presented in this part.

3.1 Diffusion models

In general, the compacted bentonite is composed of three phases, namely the solid, liquid water and gas (air and water vapor). In the simulations, the conservation mass of each phase (water or gas) is assumed. The phase exchange term thus will not be considered in the balance equations. The variables chosen for the description of the flow problem are liquid water pressure, gas pressure and temperature.

3.1.1 *Water species*

For the water species, the mass conservation equation is obtained by summing the balance equation of liquid water and water vapor. The equation includes the variation of water storage and the divergence of water flows in each phase. Considering that water vapor is a component of gaseous phase, it thus has two contributions: the advective flux of gaseous phase and the non-advective flux of the water vapor related to vapor diffusion inside the gaseous phase (Collin et al., 1999), which can be written as

$$\frac{\partial \rho_{\mathrm{w}} n S_{\mathrm{r,w}}}{\partial t} + \mathrm{div}(\rho_{\mathrm{w}} \underline{f}_{\mathrm{w}}) + \frac{\partial \rho_{\mathrm{v}} n S_{\mathrm{r,g}}}{\partial t} + \mathrm{div}(\underline{i}_{\mathrm{v}} \rho_{\mathrm{v}} \underline{f}_{\mathrm{g}}) = 0 \tag{1}$$

where ρ_{w} is the liquid water density, n is the medium porosity, $S_{\mathrm{r,w}}$ is the water degree of saturation, $\underline{f}_{\alpha}$ (α=w, g) represents the macroscopic velocity of the phase α, $\underline{i}_{\mathrm{v}}$ is the non-advective flux of the water vapor, ρ_{v} is water vapor density, $S_{\mathrm{r,g}}$ is the gas degree of saturation in volume, and t is the time. The first two items in Eq. (1) are related to liquid water, and the latter two are associated with water vapor.

The generalized Darcy's law for multiphase porous medium is adopted to simulate the motion of liquid water:

$$\underline{f}_{\mathrm{w}} = -\frac{k_{\mathrm{int}} k_{\mathrm{r,w}}}{\mu_{\mathrm{w}}} (\underline{\nabla} p_{\mathrm{w}} + g \rho_{\mathrm{w}} \underline{\nabla} y) \tag{2}$$

where p_{w} is the liquid water pressure, y is the vertical upward directed co-ordinate, g is the gravity acceleration, μ_{w} is the dynamic viscosity of the liquid water, k_{int} is the intrinsic permeability, and $k_{\mathrm{r,w}}$ is the water relative permeability.

For the pores partially filled by air, it will be more difficult to constitute pathways for water flow, thus the permeability is consequently decreased. The variation in permeability with the degree of saturation is taken into account by introducing the variable of water relative permeability $k_{\mathrm{r,w}}$.

The water vapor flow is assumed to follow Fick's diffusion law in a tortuous medium. In the study, the formulation proposed by the model of Philip and de Vries (1957) is adopted:

$$\underline{i}_{\mathrm{v}} = -D_{\mathrm{atm}} \tau_{\mathrm{v}} n S_{\mathrm{r,g}} \underline{\nabla} \rho_{\mathrm{v}} \tag{3}$$

where D_{atm} is the molecular diffusion coefficient, and τ_{v} is the tortuosity.

3.1.2 *Heat diffusion*

In the context, one unique temperature variable is adopted. It means that the temperature is assumed to be homogenous in all phases. The heat transport is related to three effects: conduction, convection and vaporization, as presented in the following equation:

$$q' = -\Gamma \underline{\nabla} T + [c_{\mathrm{p,w}} \rho_{\mathrm{w}} \underline{f}_{\mathrm{w}} + c_{\mathrm{p},\alpha} (\underline{i}_{\mathrm{a}} + \rho_{\mathrm{a}} \underline{f}_{\mathrm{g}}) + c_{\mathrm{p,v}} (\underline{i}_{\mathrm{v}} + \rho_{\mathrm{v}} \underline{f}_{\mathrm{g}})](T - T_0) + (\underline{i}_{\mathrm{v}} + \rho_{\mathrm{v}} \underline{f}_{\mathrm{g}}) L \tag{4}$$

where Γ is the medium conductivity, and $c_{\mathrm{p},\alpha}$ (α = w, v, a) represents the specific heat of phase α. In general, the thermal conductivity is dependent on the temperature and degree of saturation. For simplicity, the influence of temperature on thermal conductivity is not considered herein.

3.2 Mechanical model

The significant influence of degree of saturation on the mechanical behavior of soil has been verified by numerous experimental studies, which should be taken into account in the mechanical modeling. Based on the experimental investigations, some constitutive models were proposed (Alonso et al., 1990, 1999; Tang and Cui, 2009). The Barcelona basic model (BBM) is widely used because of its capacity of representing the main fundamental features of partially saturated soils in a consistent and unified manner. It should be noted that the expansive behavior of compacted bentonite is better represented with the modified BBM (Alonso et al., 1999) by taking into account the microstructural variation during wetting process. However, the formulation of the model is much more complicated, and some parameters are difficult to be identified. As a preliminary study, the BBM is adopted. A brief introduction to this model is also given.

3.2.1 *Yield surface*

The BBM model is based on the classic Cam-Clay model. In consideration of the influence of degree of saturation on the mechanical behavior, suction is adopted as an independent variable in this model. The plastic yield surface is thus written in three-dimensional (3D) stress space (p, q, s). For the BBM, the yield surfaces are composed of three parts. In the (p, q) space, for a given suction, the yield surface can be written as

$$q^2 - M^2 (p + p_{\mathrm{s}})(p_0 - p) = 0 \tag{5}$$

where p is the mean stress, q is the deviatoric stress, M is the slope of the critical line, p_{s} is the soil strength in extension, and p_0 is the pre-consolidation pressure. p_0 varies with the suction. The following equation is proposed, which is well known as the LC curve:

$$p_0 = p_{\mathrm{c}} \left(\frac{p_0^*}{p_{\mathrm{c}}} \right)^{\frac{\lambda(0)-k}{\lambda(s)-k}} \tag{6}$$

where p_0^* is the pre-consolidation pressure in saturated condition, p_{c} is a reference pressure, k is the elastic slope of the compressibility curve against the net mean stress, $\lambda(0)$ is the plastic slope for the saturated condition, and $\lambda(s)$ is the plastic slope of the compressibility curve against the net mean stress (Fig. 2).

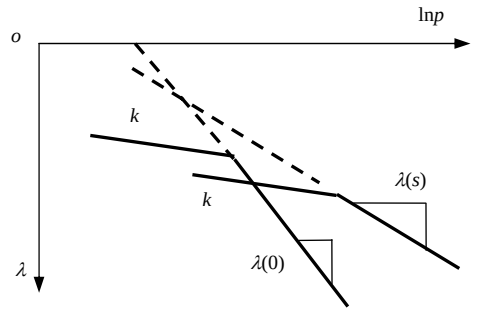

Fig. 2 Compression curve for saturated and unsaturated soil.

Under unsaturated condition, the suction contributes to stiffening the soil against the external load. Hence, the plastic slope of the compressibility curve varies with the suction. The following equation is proposed to represent this phenomenon:

$$\lambda(s)=\lambda(0)[(1-r)\exp(-\beta s)+r] \tag{7}$$

where r and β are the parameters describing the changes in soil stiffness with suction. The LC curve defines another part of the yield surface used for modeling the collapse behavior under wetting.

Numerous studies confirmed that irreversible volumetric deformation may be induced by variations in suction. Therefore, the SI yield surface, which defines the maximum previously attained value of the suction, is employed to take into account this phenomenon:

$$F_2=s-s_0=0 \tag{8}$$

where s is the suction, and s_0 represents the maximum historic suction submitted to the soil.

3.2.2 *Hardening law*

The evolution of yield surfaces is assumed to be controlled by the total plastic volumetric strain ε_v^p. Two hardening laws define the evolution of state variables p_0 and s_0 with the irreversible strain:

$$\mathrm{d}p_0^*=\frac{(1+e)p_0^*}{\lambda(0)-k}\mathrm{d}\varepsilon_v^p \tag{9}$$

$$\mathrm{d}s_0=\frac{(1+e)(s_0+P_{at})}{\lambda_s-k_s}\mathrm{d}\varepsilon_v^p \tag{10}$$

where e is the porosity of the soil; P_{at} is the atmospheric pressure; λ_s and k_s are the plastic and elastic stiffness parameters for suction variation, respectively.

4 Numerical simulations

4.1 Experimental system

The China-mock-up is designed as a vertical steel tank of 0.9 m inner diameter, and 2.2 m high with a central electrical heater of 0.3 m in diameter, which substitutes a loaded waste canister. Groundwater flow is simulated by the hydration tubes installed at the outer boundary of buffer. The steel tank is filled by compacted GMZ bentonite blocks, as illustrated in Fig. 3.

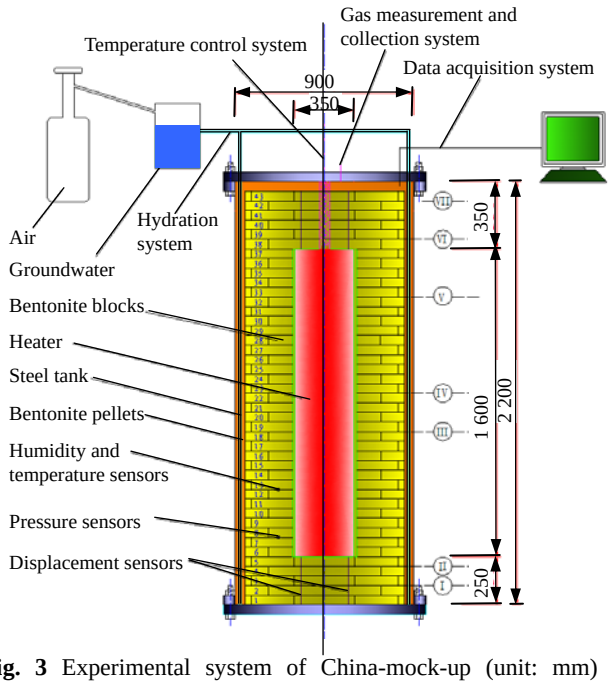

Fig. 3 Experimental system of China-mock-up (unit: mm) (Wang, 2010).

According to the experimental program, the test will be carried out by applying a constant temperature of 90 °C to buffer material by the electrical heater and a constant water pressure of 2 MPa to the outer boundary by the hydration tubes. The total duration is around 3 years. A number of sensors are installed in the compacted blocks to measure the physico-mechanical variables, including the stress, the displacement, the water pressure, the humidity and the temperature.

4.2 Geometry and boundary conditions

A 2D-axisymetric finite element simulation is realized with the help of the software LAGAMINE. The geometry and boundary conditions are illustrated in Fig. 4.

For simplicity, the steel tank is neglected to address the problem in the numerical test. The fixed horizontal/vertical displacement is imposed on the nodes in contact with the steel and the heating is simulated by imposing the temperature on the nodes in contact with the heater. The hydration influence is modeled by increasing water pressure on the nodes of outer boundary. The convection transfer between the GMZ bentonite and the atmosphere is simulated thanks to frontier thermal elements. In the simulations, air flow

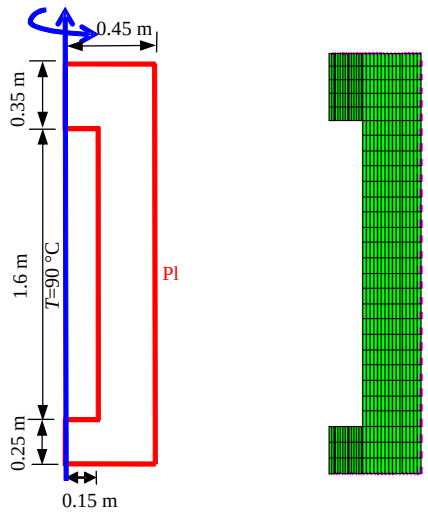

Fig. 4 Boundary conditions and the meshes.

is not considered, whereas the vapor diffusion is assumed.

The system is initially at temperature of 20 °C. The gas pressure is assumed to be constant in order to have a better numerical convergence. The compacted GMZ bentonite has an initial water saturation of 48% and a void ratio of 0.57. According to the water retention curve determined, a suction of 80 MPa is initially employed. As aforementioned, the dissolved air will not be taken into account.

Following the experimental procedure, the numerical simulations are divided into two phases: the temperature on the boundary connected to the heater and the water pressure on the outer boundary are increased to 90 °C and 2 MPa, respectively, in 10 hours. In the following, the boundary conditions applied previously are kept constant in 3 years.

4.3 Determination of THM parameters

4.3.1 *Hydro-thermal properties*

Among the hydro-thermal properties, the water retention curve and permeability are considered as the key factors on the water intake volume and the final degree of saturation. Measured data of water content in function of suction is available (Chen et al., 2006). The relation between suction and water saturation is adopted in the study:

$$S_{\mathrm{r,\,w}} = S_{\mathrm{r,\,res}} + a_3 \frac{S_{\mathrm{r,\,u}} - S_{\mathrm{r,\,res}}}{a_3 + (a_1 s)^{a_2}} \tag{11}$$

where $S_{\mathrm{r,\,u}}$ is the maximum degree of saturation in the soil, $S_{\mathrm{r,\,res}}$ is the residual degree of saturation for a very high value of suction, and a_i $(i=1-3)$ is the parameter.

Values of $S_{\mathrm{r,\,u}}$ and $S_{\mathrm{r,\,res}}$ determined in test are 1.0 and 0.1, respectively. Calibration of this function on measured data gives the values of the following parameters: a_1=3.5×10^{-6} Pa^{-1}, a_2=0.8, a_3=90. Water retention curve of the GMZ bentonite is illustrated in Fig. 5.

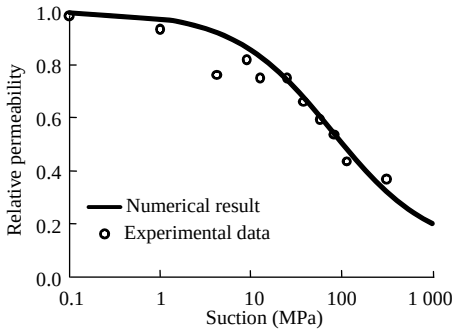

Fig. 5 Water retention curve of the GMZ bentonite.

Relative permeability curves are determined based on the experimental investigation (Ye et al., 2009b), as shown in Fig. 6. The intrinsic permeability k_{int}= 2.0×10^{-21} m^2 is chosen according to the experimental data. Thus, we have

$$k_{\mathrm{r,\,w}} = \frac{(S_{\mathrm{r,\,w}} - S_{\mathrm{r,\,res}})^4}{(S_{\mathrm{r,\,u}} - S_{\mathrm{r,\,res}})^4} \tag{12}$$

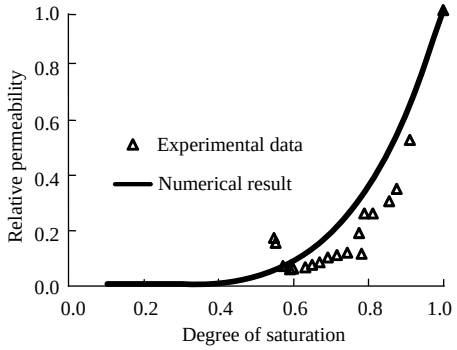

Fig. 6 Variation of relative permeability in function of degree of saturation.

A linear relation is adopted to describe the variation in thermal conductivity with degree of saturation, as shown in Fig. 7. Table 1 summarizes the other parameters of the hydraulic and thermal properties.

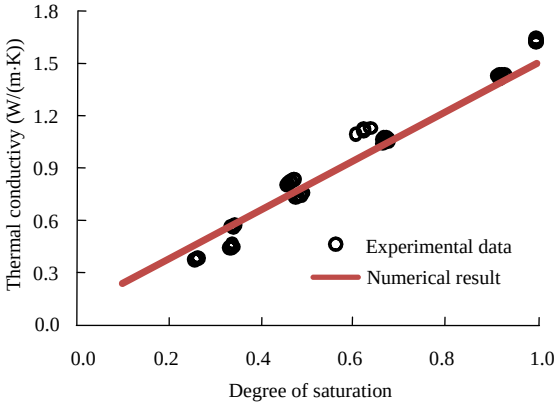

Fig. 7 Variation of thermal conductivity with degree of saturation.

Table 1 Parameters of the flow model.

Grain density, ρ_s (kg/m^3)	Grain specific heat, $c_{p,s}$ (J/(kg·K))	Water density, ρ_w (kg/m^3)	Water dynamic viscosity, μ_w (Pa·s)	Water specific heat, $c_{p,w}$ (J/(kg·K))	Air density, ρ_a (kg/m^3)
1.6×10^3	2.6	1.0×10^3	1.009×10^{-3}	4.18×10^3	1.205

Air dynamic viscosity, μ_a (Pa·s)	Air specific heat, $c_{p,a}$ (J/(kg·K))	Water vapour specific heat, $c_{p,v}$ (J/(kg·K))	Latent heat of vaporization, L (J/kg)	Tortuosity, τ
1.80×10^{-5}	1.0×10^3	1.90×10^3	2.50×10^6	0.1

4.3.2 *Mechanical parameters*

The mechanical loading test at constant suction and temperature (Cui et al., 2011) revealed that elastic stiffness parameter k and plastic stiffness parameter $\lambda(s)$ of the GMZ bentonite increase with decrease in suction but are independent of the temperature changes. The effect of temperature on the yield stress p_0 of the GMZ bentonite is found to be insignificant. For simplicity, a constant value of the elastic stiffness parameter k is adopted. The parameters γ and β, which define the variation of $\lambda(s)$ with suction, are determined based on experimental data (Fig. 8).

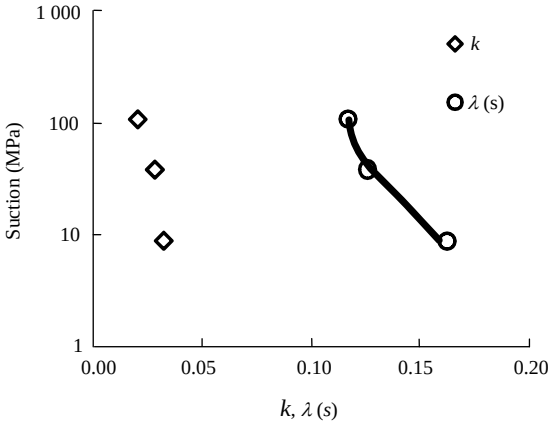

Fig. 8 Variation in k and $\lambda(s)$ with suction.

The LC curve describes the evolution of p_0 with suction, which depends on k, $\lambda(s)$ and p_c. The reference pressure p_c cannot be directly determined, thus a calibration procedure is adopted. The stiffness parameters k_s and λ_s define the volumetric strain changes induced by suction. According to the experimental study, a volumetric strain of 32.4% is obtained when the suction is decreased from 110 to 9 MPa. Considering that the volumetric strain is induced in a wetting procedure (inferior to the maximum historic suction), it can be considered as elastic volumetric strain. Therefore, a value of 0.07 is determined for k_s. Due to the lack of experimental data, an average value of $\lambda(s) = 0.25$ obtained from other types of bentonites is taken in the simulations (Collin et al., 1999). Based on the water retention curve, s_0 can be fixed from the initial degree of saturation.

The dependence of these parameters on the stress state generated in the soil sample is not taken into account. The values of parameters used in the simulations are summarized in Table 2.

Table 2 Parameters employed in mechanical model.

Saturated virgin compression index, $\lambda(0)$	Elastic compression index, k	Saturated pre-consolidation pressure, p_0^* (MPa)	Elastic stiffness index upon suction, k_s	Plastic stiffness index upon suction, λ_s
0.18	0.027	0.6	0.08	0.25

Maximum value of the suction, s_0 (MPa)	Reference stress, p_c (MPa)	Ratio $\lambda(s)/\lambda(0)$ for high suction	Parameters to control the increase in stiffness with suction (MPa)
80	0.45	0.65	0.045

4.4 Predictive results and analysis

With the given parameters, the simulations of experimental process are carried out. The evolution of temperature vs. time in the lateral direction is illustrated in Fig. 9. As defined in boundary conditions, the temperature is kept at 90 °C on the nodes connected to the electric heater. At the beginning, the temperature of the compacted bentonite increases significantly, especially in the first month. Thanks to the frontier thermal elements, the temperature on the exterior boundary also increases with time.

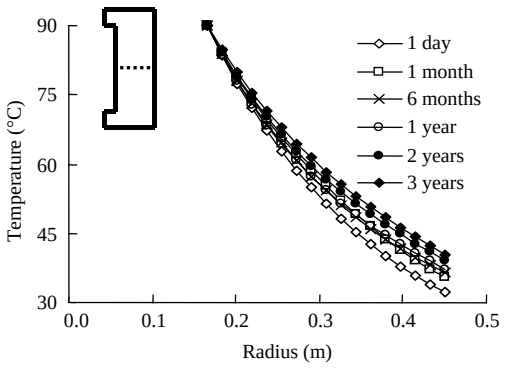

Fig. 9 Evolutions of temperature vs. time (along the dotted line).

The compacted bentonite is progressively saturated by the water inflow (Fig. 10), which is in an opposite direction to heat flow. However, due to the extremely low permeability and evaporation, the compacted bentonite close to the heater still stays partially saturated after 3 years (Fig. 11).

Fig. 10 Water flow at the end of simulations (3 years later).

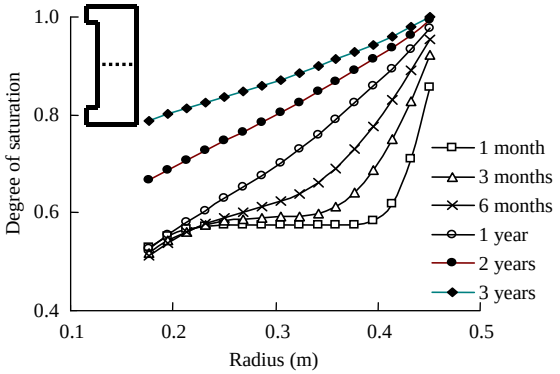

Fig. 11 Distribution of degree of saturation with time.

In terms of suction, due to the saturation process by water penetration, the suction is decreased globally (Fig. 12). It is interesting that a more significant suction (100 MPa) than the initial value (80 MPa) can be noticed at the beginning. It indicates that the bentonite is desaturated in this period of time.

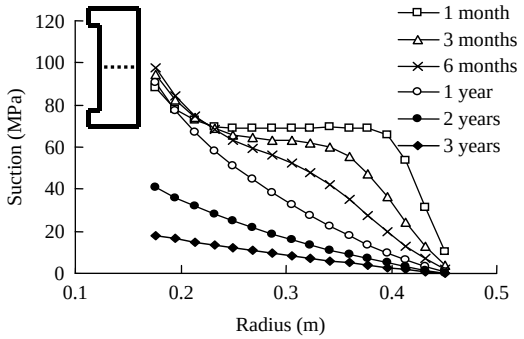

Fig. 12 Suction-time evolution in lateral direction.

This phenomenon is well presented in Fig. 13, in which the suction responses of the three points (*A*, *B*, *C*) in lateral direction are illustrated. It is noticed that at point *A*, the suction increases at first, and then decreases. This desaturation-saturation process can be attributed to the evaporation phenomenon, generated by high temperature of the electrical heater. In Fig. 14, water vapor is generated and transported towards outer boundary in the field exposed to high temperature. The desaturation process indicates that at the beginning, the evaporation phenomenon is dominant compared to the saturation effect induced by the water inflow. This phenomenon is also observed in other experiments, like the canister retrieval test (CRT) carried out by SKB (Akesson et al., 2010).

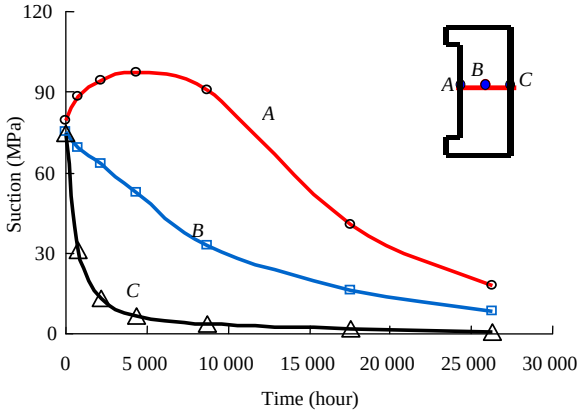

Fig. 13 Suction responses of the three points in lateral direction.

Fig. 14 Vapor flows at the end of simulations (3 years later).

The predicted water pressure with time is illustrated in Fig. 15. It is noticed that in the field exposed to high temperature, the suction is more significant, especially for the area close to the upper surface and the bottom of the electrical heater. At the end of the simulations (3 years later), a suction of around 59 MPa is reached in this field. This result seems reasonable considering that the field is far from the outer boundary. Moreover, the evaporation generated by high temperature is also more significant.

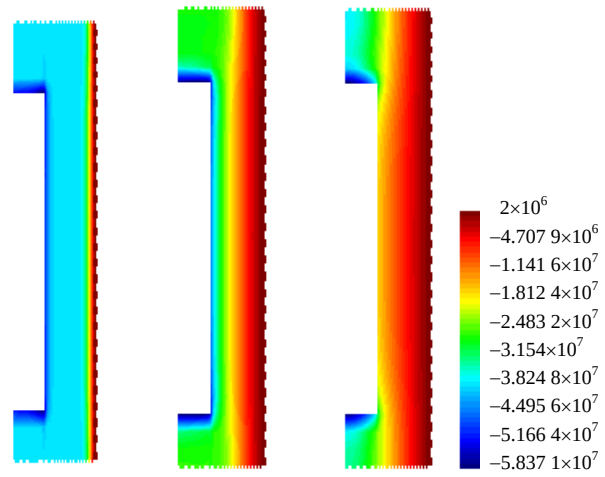

(a) 1 month. (b) 1 year. (c) 3 years.

Fig. 15 Distribution of water pressure (unit: Pa).

The swelling pressure variation with time at point *A* with coordinates *r*=0.15 m and *z*=0.123 m is illustrated in Fig. 16.

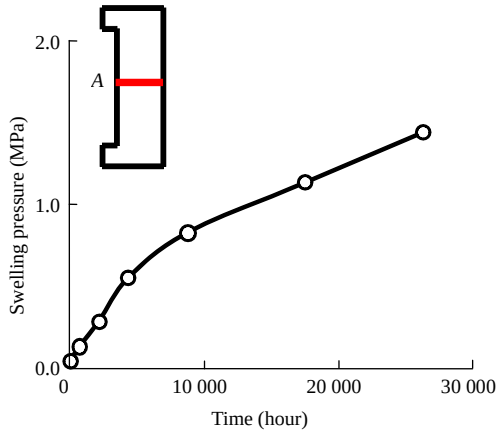

Fig. 16 Swelling pressure evolution at point *A*.

It can be noticed that the swelling pressure increases rapidly at the beginning, and a value of 1.5 MPa is obtained after 3 years, which seems relatively limited. It can be attributed to two aspects: first, considering the saturation process is not completed, the maximum value is not yet reached; on the other hand, the expansion strain induced by the variation in microstructure of bentonite during wetting process is not considered in the BBM.

5 Parametric studies

In order to evaluate the influence of the thermo-hydraulic properties on the experiments, parametric studies of permeability and water retention curve are realized in this context.

5.1 Permeability

Three values of intrinsic permeability are studied, namely 2×10^{-21}, 4.5×10^{-21} and 6×10^{-21} m^2. The distribution of temperature in three cases (Fig. 17) indicates that temperature increases more rapidly with increase in permeability.

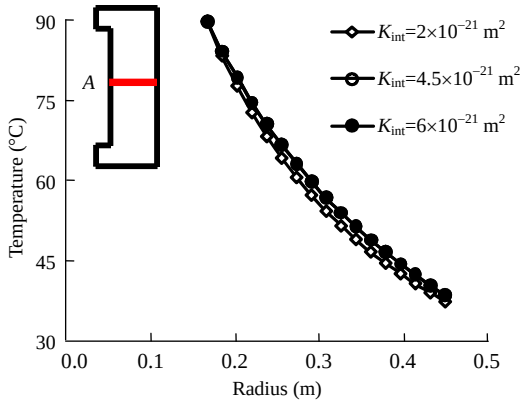

Fig. 17 Distribution of temperature after 1 year for three cases.

This can be explained by the dependence of the thermal conductivity on degree of saturation. In addition, the convective heat transport induced by the water inflow is another factor. However, this influence seems limited and the difference in temperature vanishes after 2 years. At the end of the simulations (3 years later), almost no difference can be identified.

Increasing permeability also brings a more rapid saturation process. In Fig. 18, the desaturation-saturation process vanishes with the increasing permeability at point *A*. It means that in the field exposed to high temperature, water inflow is dominant compared to evaporation at the beginning for a higher permeability.

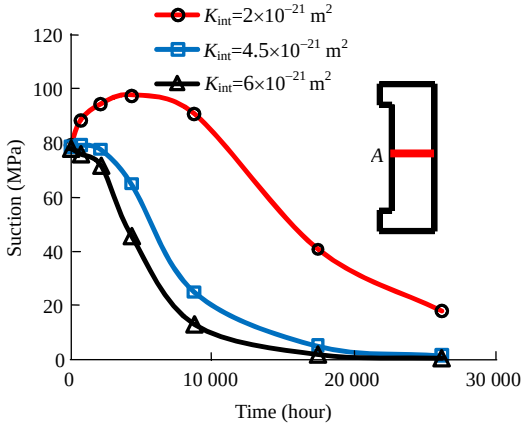

Fig. 18 Variation in suction with time at point *A* for different cases of permeability.

Due to the accelerated saturation process by higher permeability, the swelling pressure increases more significantly, as shown in Fig. 19.

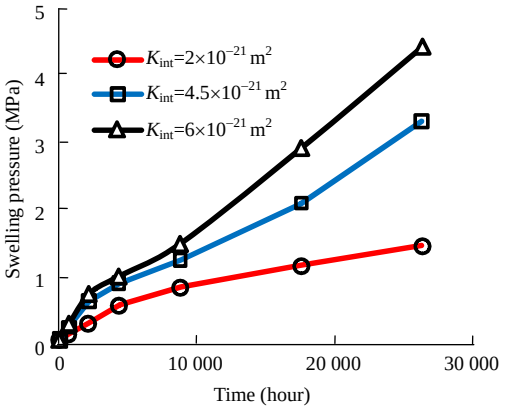

Fig. 19 Variation in swelling pressure with time for three cases.

5.2 Water retention curve

In Fig. 20, three water retention curves are investigated. The WRC1 is the water retention curve determined from experimental data of the GMZ bentonite. In the simulations, the same initial suction of 80 MPa is applied.

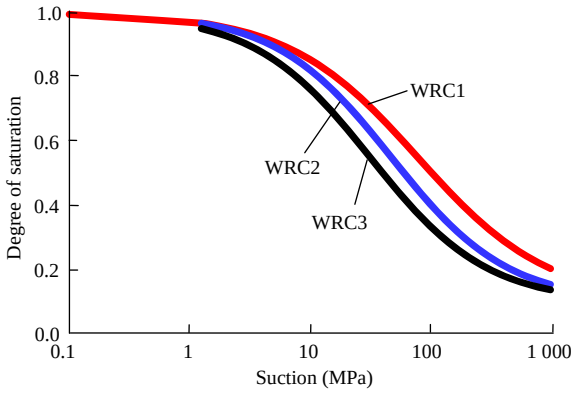

Fig. 20 Three WRCs in the simulations.

The predictive results indicate a significant influence of WRC on the distribution of temperature. Compared to the result of WRC1, the temperature of other cases is much lower (Fig. 21). This can be also explained by the dependence of thermal conductivity on degree of saturation. As illustrated in Fig. 20, the same suction value corresponds to a lower degree of saturation for WRC3, which means a smaller thermal conductivity and relative permeability. Therefore, the desaturation-saturation process takes more time at point *A* for WRC2 and WRC3 (Fig. 22).

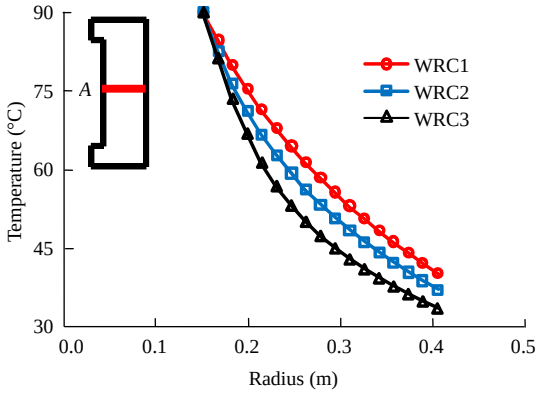

Fig. 21 Distribution of temperature after 1 year for three WRCs.

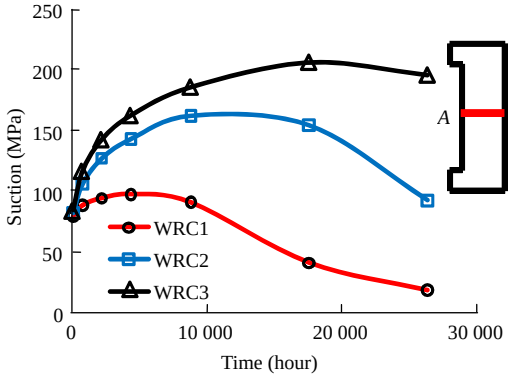

Fig. 22 Variation in suction with time at point *A* for three WRCs.

Due to the slower saturation process, the generated swelling pressure of WRC2 and WRC3 is also smaller than that of WRC1 (Fig. 23).

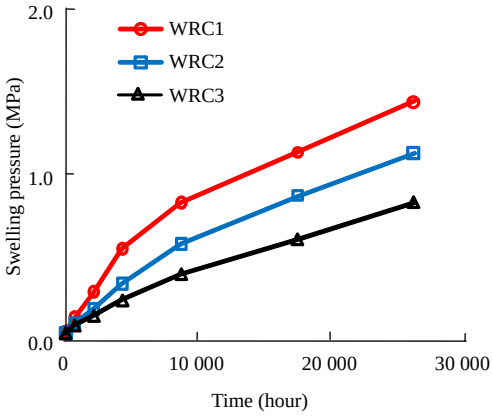

Fig. 23 Variation in swelling pressure with time for three WRCs.

6 Conclusions

In the paper, a THM model is proposed to reproduce the complex coupling behaviors of the compacted GMZ bentonite. With the proposed model, numerical simulations of the China-mock-up test are realized. According to the discussion on the predictive results, some conclusions are drawn and summarized as follows:

(1) Due to the extremely low permeability, the saturation process of the compacted GMZ bentonite seems very slow. According to the numerical results, in the field near-by the electrical heater, the compacted

bentonite is not fully saturated after 3 years.

(2) A desaturation-saturation process is noticed in field near-by the electrical heater, which can be explained by the competitive mechanism between the drying effect induced by the high temperature, and the saturation process by water penetration.

(3) The parametric analysis indicates that the behavior of the compacted GMZ bentonite is highly sensitive to its thermal and hydraulic properties, especially to the water retention curve and the permeability.

(4) Based on the qualitative analysis of the predictive results, it is suggested that the proposed model is capable of reproducing the principal coupled THM behaviors of the compacted GMZ bentonite.

As a qualitative analysis of the predictive results, the numerical study realized only can be considered as a preliminary verification of the proposed model. With the progress of the experimental test, further study is needed.

Acknowledgments

The authors would like to thank Prof. Cui and Dr. Chen for providing experimental data and useful discussions.

References

Akesson M, Borgesson L, Kristensson O. THM modeling of buffer, backfill and other system components: critical processes and scenarios. Stockholm: SKB Technical Report, 2010.

Alonso E E, Gens A, Josa A. A constitutive model for partially saturated soils. Geotechnique, 1990, 40 (3): 405–430.

Alonso E E, Vaunat J, Gens A. Modeling the mechanical behavior of expansive clays. Engineering Geology, 1999, 54 (1): 173–183.

Charlier R. Approach unifiée de quelques problèmes non linéqires de mécanique des milieux continus par la méthode des éléments finis. Ph.D. Thesis. Liège: Université de Liège, 1987.

Chen Bao, Qian Lixin, Ye Weimin, Cui Yujun, Wang Ju. Soil-water characteristic curves of Gaomiaozi bentonite. Chinese Journal of Rock Mechanics and Engineering, 2006, 25 (4): 788–793 (in Chinese).

Collin F, Li X L, Radu J P, Charlier R. Thermo-hydro-mechanical coupling in clay barriers. Engineering Geology, 1999, 54 (2/3): 173–183.

Cui Yujun, Tang Anhminh, Qian Lixin, Ye Weimin, Chen Bao. Thermal-mechanical behavior of compacted GMZ bentonite. Soils and Foundations, 2011, 51 (6): 1 065–1 074.

Liu Yuemiao, Cai Meifeng, Wang Ju, Wen Zhijian. Compressibility of buffer material for HLW disposal in China. Uranium Geology, 2007a, 23 (2): 91–95 (in Chinese).

Liu Yuemiao, Cai Meifeng, Wang Ju. Thermal properties of buffer material for high-level radioactive waste disposal. Chinese Journal of Rock Mechanics and Engineering, 2007b, 26 (Supp. 2): 3 891–3 896 (in Chinese).

Philip J R, de Vries D A. Moisture movement in porous materials under temperature gradients. Transactions, American Geophysical Union, 1957, 38 (2): 222–232.

Tang A M, Cui Y J. Modeling the thermo-mechanical volume change behaviour of compacted expansive clays. Geotechnique, 2009, 59 (3): 185–195.

Wang Ju. High-level radioactive waste disposal in China: update 2010. Journal of Rock Mechanics and Geotechnical Engineering, 2010, 2 (1): 1–11.

Wang Ju, Chen Weiming, Su Rui, Guo Yonghai, Jin Yuanxin. Geological disposal of high-level radioactive waste and its key scientific issues. Chinese Journal of Rock Mechanics and Engineering, 2006, 25 (4): 801–812 (in Chinese).

Wen Zhijian. Selection and basic properties of China's buffer materials for high level radioactive waste repository. Acta Petrologica et Mineralogical, 2005, 24 (6): 584–588 (in Chinese).

Wen Zhijian. Physical property of China's buffer material for high-level radioactive waste repositories. Chinese Journal of Rock Mechanics and Engineering, 2006, 25 (4): 794–800 (in Chinese).

Wersin P, Johnson L H, McKinley I G. Performance of the bentonite barrier at temperature beyond 100 °C: a critical review. Physics and Chemistry of the Earth, 2007, 32 (8/14): 780–788.

Ye Weimin, Schanz T, Qian Lixin, Wang Ju, Rifin A. Characteristics of swelling pressure of densely compacted Gaomiaozi bentonite GMZ01. Chinese Journal of Rock Mechanics and Engineering, 2007, 26 (Supp. 2): 3 861–3 865 (in Chinese).

Ye Weimin, Wan Min, Chen Bao, Chen Yonggui, Cui Yujun, Wang Ju. Effect of temperature on soil-water characteristics and hysteresis of compacted Gaomiaozi bentonite. Journal of Central South University of Technology, 2009a, 16 (5): 821–826.

Ye W M, Cui Y J, Qian L X, Chen B. An experimental study of the water transfer through confined compacted GMZ bentonite. Engineering Geology, 2009b, 108 (3/4): 169–176.

Ye Weimin, Chen Yonggui, Chen Bao, Wang Qiong, Wang Ju. Advances on the knowledge of the buffer/backfill properties of heavily compacted GMZ bentonite. Engineering Geology, 2010, 116 (1/2): 12–20.